

Fast Approximation of Optimal Perturbed Many-Revolution Multiple-Impulse Transfers via Deep Neural Networks

Yue-he Zhu^{*}, Ya-zhong Luo[†]

National University of Defense Technology, 410073, Changsha, People's Republic of China

Abstract The design of perturbed multiple-impulse-based multitarget rendezvous missions requires a method to quickly and accurately approximate the optimal perturbed many-revolution multiple-impulse transfer between any two rendezvous targets. The approximation of an optimal transfer refers to the estimation of the optimal transfer velocity increments. In this paper, a deep neural network (DNN)-based method is proposed for quickly approximating optimal perturbed many-revolution multiple-impulse transfers. This kind of transfers is divided into three types according to the initial and final states of the departure body and rendezvous target. An efficient database generation method combined with a reliable optimization approach is developed to generate each type of transfers. Three regression DNNs are trained individually and applied to estimate the optimal velocity increments of the transfers belonging to each type. The simulation results show that the well-trained DNNs are capable of quickly estimating the optimal velocity increments with a relative error of less than 3% for all the three types of transfers. The tests on two debris transfer chains further show the superiority of the DNN-based method for application to the design of perturbed multiple-impulse-based multitarget rendezvous missions.

I. Introduction

^{*} Ph.D. Candidate, College of Aerospace Science and Engineering; zhuyuehe@nudt.edu.cn.

[†] Professor, College of Aerospace Science and Engineering; luoyz@nudt.edu.cn. Senior Member AIAA.

The design of a multitarget rendezvous mission, in which the core task is to solve a sequence-undetermined global trajectory optimization problem (GTOP) that resembles the moving-target traveling salesman problem (TSP), is usually challenging. Compared with the classical moving-target TSP and its variants [1], a perturbed multiple-impulse-based GTOP such as the problem of the ninth edition of the Global Trajectory Optimization Competition (GTOC-9) [2] is more difficult to solve because achieving the optimal velocity increments of a perturbed many-revolution multiple-impulse transfer is much more complex and time consuming than calculating the distance between two cities. Huge numbers of possible transfers are required to be evaluated in sequence optimization, and it is apparently impracticable to optimize the velocity increments for each transfer while optimizing the rendezvous sequence. Fast estimation of the optimal velocity increments for each transfer is necessary for the design of perturbed multiple-impulse-based multitarget rendezvous missions.

Due to the difficulty in achieving the optimal transfer velocity increments, few studies focused on perturbed many-revolution multiple-impulse transfers previously, and there was a lack of an efficient method that can quickly and accurately estimate the optimal velocity increments of this kind of transfers. Drawn by the problem of GTOC-9, several analytical methods for estimating the optimal velocity increments of this kind of transfers emerged [3-7]. These methods were developed by the participants of GTOC-9, and most of these methods estimate the optimal velocity increments by selectively adding or taking the root-sum-square of individual velocity increments required for matching the semi-major axis, eccentricity, inclination, right

ascension of the ascending node (RAAN) and phase of the rendezvous target. Without complex calculation, the result can be quickly obtained. However, the approximating performance is usually not satisfactory. The relative estimation error can be up to 30% for some methods [6-7]. The optimal transfer chain can hardly be found if applying an estimator with such a large error in sequence optimization even if the global search ability is powerful enough. A more reliable approximation method is required for the design of perturbed multiple-impulse-based multitarget rendezvous missions.

From the mathematical point of view, the estimation of the optimal transfer velocity increments is essentially a regression problem. Numerous studies have shown that machine learning-based (ML-based) methods own the superiority on solving regression problems as long as relevant learning features are well identified and training samples are sufficient [8]. The representative ML-based works that are related to this study are noteworthy. Shang and Liu [9] applied a Gaussian process regression model to evaluate the accessibility of main-belt asteroids instead of optimizing the transfer trajectories for the candidate asteroids one by one. Much simulation time was saved, and the estimated results were close to the numerical optimal solutions. Zhu et al. [10] expanded Shang and Liu's work to the evaluation of round-trip transfers for manned main-belt asteroids exploration mission, and the estimation error was reduced to less than 1.2%. More relatedly, Hennes et al [11] studied the fast approximation of optimal low-thrust hop between main-belt asteroids for the design of multi-asteroid visiting missions. Several state-of-the-art ML models were employed to estimate the optimal final mass of the spacecraft, and the estimation accuracy was significantly

improved compared with the traditional method. Mereta et al [12] promoted Daniel's work to a more complicated case with multiple-revolution transfers in the near earth regime and achieved similar results. The success of the above applications inspires our attempt to apply an ML-based method to estimate the optimal velocity increments of perturbed many-revolution multiple-impulse transfers.

A good learning model is required for the estimation of the optimal transfer velocity increments. As an important member of the ML family, the deep neural networks (DNNs), which refer to the artificial neural networks with more than one hidden layer [13], have increasingly been popular in recent years. A DNN with an appropriate network structure and activation function is expected to have a stronger approximation ability than traditional ML models [14], especially for the complex classification and regression problems. The significant achievements of AlphaGo [15] and OpenAI [16] have attracted large amounts of attention on DNNs. The DNN-based researches that have emerged recently in aerospace fields are also noteworthy. Sánchez-Sánchez [17-18] applied DNNs to learn the solution of inverted pendulum stabilization and optimal landing problems, so that real-time on-board trajectory planning could be achieved. Maggiori et al. [19] proposed a fully convolutional network architecture by analyzing a state-of-the-art model and solving its concerns by construction. Their overall framework showed that convolutional neural networks could be used end-to-end to process massive satellite images and provide accurate pixelwise classifications. Furfaro et al. [20] validated that a deep Recurrent Neural Network architecture was capable of predicting the fuel-optimal thrust from sequence

of states during a powered planetary descent. Peng and Bai [21] showed that a well-trained DNN could also be combined with physics-based models to improve the orbit prediction accuracy by learning space environment information from large amounts of observed data. Owing to the powerful approximation ability, DNNs are applied as the learning model for the approximation of optimal perturbed many-revolution multiple-impulse transfers in this paper.

For better estimating the optimal velocity increments of this kind of transfers, how the optimal velocity increments vary with the increase of the initial RAAN difference and transfer time is first studied. It is suggested that this kind of transfers should be divided into three types, and three regression DNNs are required to estimate the optimal velocity increments for each transfer type. The most appropriate learning features and network scale (i.e., the number of nodes and hidden layers) of these regression DNNs are investigated. The comparison between the DNN-based method and two typical analytical methods are presented, and two debris transfer chains are further applied to validate the superiority of the DNN-based method for approximating optimal perturbed many-revolution multiple-impulse transfers.

The contributions of this paper are summarized as follows. 1) An efficient optimization approach for achieving near-optimal perturbed many-revolution multiple-impulse transfers is proposed. 2) How the optimal velocity increments of a perturbed many-revolution multiple-impulse transfer vary with the increase of the initial RAAN difference and transfer time is analyzed, and this study first finds that there is a lower bound of the optimal velocity increments for this kind of transfers. 3)

A DNN-based method for quickly and accurately approximating optimal perturbed many-revolution multiple-impulse transfers is developed, and this method is verified to be practical for application to the design of perturbed multiple-impulse-based multitarget rendezvous missions.

The remainder of this paper is organized as follows. Section II briefly describes the perturbed multiple-impulse trajectory optimization model. Section III introduces the optimization approach for achieving near-optimal perturbed many-revolution multiple-impulse transfers and validates the efficiency of the approach. Section IV studies how the optimal velocity increments of this kind of transfers vary with the increase of the initial RAAN difference and transfer time. Section V presents the complete process of the DNN-based method for estimating the optimal transfer velocity increments. Detailed simulations for determining the most appropriate learning features and network scales of the regression DNNs and the demonstration of the superiority of the DNN-based method for estimating the optimal transfer velocity increments are given in Section VI. Conclusions are drawn in Section VII.

II. Perturbed Multiple-Impulse Trajectory Optimization Model

A. Orbital dynamics

The motion of a spacecraft flying around the Earth can be modeled as

$$\begin{aligned}\dot{\mathbf{r}} &= \mathbf{v} \\ \dot{\mathbf{v}} &= -\frac{\mu}{r^3} \mathbf{r} + \mathbf{a}_p\end{aligned}, \tag{1}$$

where \mathbf{r} and \mathbf{v} are the position and velocity in geocentric ecliptic reference frame; μ refers to the gravitational parameter; \mathbf{a}_p denotes the perturbation acceleration

caused by the factors such as nonspherical gravity and atmospheric drag. Only the secular effect of J2 perturbation is taken into account in this study. For a spacecraft that is described by means of the osculating orbital elements, the state of the spacecraft at any epoch t can be computed as

$$\begin{cases} a = a_0, \quad e = e_0, \quad i = i_0 \\ \Omega = \Omega_0 - \frac{3}{2} J_2 \left(\frac{R_E}{p} \right)^2 n \cos i (t - t_0) \\ \omega = \omega_0 + \frac{3}{4} J_2 \left(\frac{R_E}{p} \right)^2 n (5 \cos^2 i - 1) (t - t_0) \\ M = M_0 + \left[n + \frac{3}{4} J_2 \left(\frac{R_E}{p} \right)^2 n \sqrt{1 - e^2} (3 \cos^2 i - 1) \right] (t - t_0) \end{cases}, \quad (2)$$

where J_2 denotes the magnitude of the J2 perturbation and R_E denotes the equatorial radius of the Earth; $p = a(1 - e^2)$ and $n = \sqrt{\mu/a^3}$ are the semilatus rectum and mean motion, respectively. Once the initial state $\{a_0, e_0, i_0, \Omega_0, \omega_0, M_0, t_0\}$ and the flight time Δt are given, the osculating orbital elements at $t = t_0 + \Delta t$ is determined and the corresponding position and velocity can be directly obtained.

B. Optimization model

There are two kinds of design variables in the multiple-impulse rendezvous trajectory optimization problem. The first kind refers to the maneuver times of all the impulse, which are expressed as

$$X_1 = T_i, \quad i = 1, 2, \dots, n, \quad (3)$$

where n is the total number of the maneuvers. The second kind refers to the first $n-2$ impulses, which are expressed as

$$X_2 = \Delta V_i, \quad i = 1, 2, \dots, n-2, \quad (4)$$

where $\Delta\mathbf{V}_i = [\Delta V_{ix}, \Delta V_{iy}, \Delta V_{iz}]$ is the i^{th} impulse vector. Once \mathbf{X}_1 and \mathbf{X}_2 are determined, the spacecraft can be propagated from T_1 to T_{n-1} base on the dynamic model presented above and the last two impulses can be computed by solving a two-point boundary-value problem (TPBVP). The goal of the problem is to minimize the total velocity increments:

$$J = \min \sum_{i=1}^n \|\Delta\mathbf{V}_i\| \quad (5)$$

For a multiple-impulse rendezvous trajectory optimization problem with maximum transfer time ΔT_{\max} , all the variables in Eq. (3) must be limited to the range of $[0, \Delta T_{\max}]$. To avoid dealing with the constraints of the maneuver time sequence during optimization, the variables in Eq. (3) is modified as

$$\mathbf{X}_i = \eta_i, \quad i = 1, 2, \dots, n, \quad (6)$$

$$\begin{cases} \eta_i = T_i / T_{i+1}, & i = 1, 2, \dots, n-1 \\ \eta_n = T_n / \Delta T_{\max} \end{cases}, \quad (7)$$

where $\eta_i (i = 1, 2, \dots, n)$ are all limited to the range of $[0, 1]$. By this modification, the constraints of the maneuver times are always satisfied and a multiple-impulse transfer can be obtained as long as the terminal position and velocity constraints are satisfied:

$$\begin{cases} \|\mathbf{r}_{cf} - \mathbf{r}_{tf}\| \leq \varepsilon_r \\ \|\mathbf{v}_{cf} - \mathbf{v}_{tf}\| \leq \varepsilon_v \end{cases}. \quad (8)$$

$\mathbf{r}_{cf}, \mathbf{v}_{cf}$ and $\mathbf{r}_{tf}, \mathbf{v}_{tf}$ are the final states of the spacecraft and the rendezvous target, respectively; ε_r and ε_v are the acceptable position and velocity errors.

III. Perturbed Many-Revolution Multiple-Impulse Trajectory Optimization Approach

This study aims to develop a DNN-based method for approximating optimal perturbed many-revolution multiple-impulse transfers. Large numbers of training samples are required, and the quality of the training samples, which refers to the optimality of the transfers, must be guaranteed because it significantly influences the approximating performance. In this section, the optimization approach for achieving near-optimal solutions and the validation for the efficiency of the approach are presented.

A. Optimization approach

Prussing [22] has reported that the maximum impulse number required for the optimal coplanar rendezvous problem is four. In this study, the impulse number n is set to five because numerous simulations show that further enlarging the impulse number contributes little to the decrease of the total velocity increments but greatly increases the optimization difficulty.

The crucial step for achieving a constraint-satisfied multiple-impulse transfer is to solve the TPBVP between the last two impulses. Solving a two-body TPBVP is very easy by using either a classical Lambert algorithm [23] or a multiple-revolution Lambert algorithm [24]. However, it is difficult to solve the perturbed TPBVP directly. In this study, we apply a two-step approach to optimize the perturbed many-revolution multiple-impulse rendezvous trajectory. The process of the approach is illustrated in Figure 1. Firstly, the orbital dynamics between the last two impulses are replaced with the two-body model and a classical Lambert algorithm is used to solve the two-body

TPBVP. Note that the two-body model is also used to propagate the rendezvous target from T_{n-1} to T_n . An improved differential evolution (DE) algorithm [25] is applied to obtain the initial solution that consists of $n-1$ perturbed transfer legs and a two-body transfer leg. Then the orbital dynamics between the last two impulses are returned to the perturbed model and a sequential quadratic programming (SQP) algorithm follows to achieve the perturbed solution based on the initial solution. The transfer leg between the last two impulses is limited to one revolution to avoid the unsuccessful convergence of the SQP caused by the excessive terminal difference between the initial solution and the perturbed one.

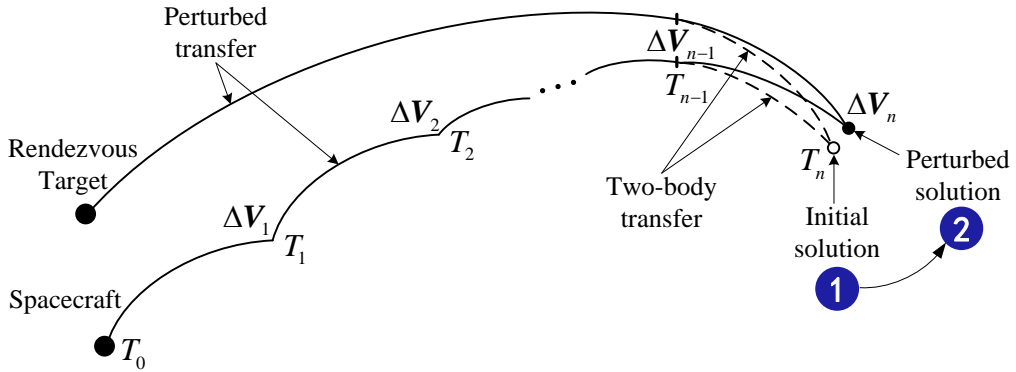


Fig. 1 Two-step approach for obtaining the perturbed multiple-impulse rendezvous solution

Due to the interference of huge numbers of local optima and the stochasticity of evolutionary algorithm, the optimality cannot be guaranteed by running only one time for each rendezvous case. In this study, 100 independent runs are implemented for each case and the best solution of the 100 runs is determined as the optimal solution.

B. Validation for the efficiency of the approach

In the two-step approach, the transfer leg between the last two impulses is limited to one revolution. Note that the original search space is actually narrowed, and the optimal solution may be missed with such a limitation. The influence of the limitation

on achieving optimal many-revolution multiple-impulse transfers is investigated and the quality of the best solution that is selected from 100 independent runs is verified.

Yang et al. [26] have developed a method based on the homotopic perturbed Lambert algorithm to solve this kind of optimization problem. By introducing a set of middle target points along the position offset vector and a new targeting technique, the homotopy-based Lambert algorithm is capable of solving perturbed multiple-revolution TPBVP, and the perturbed solution can be achieved directly without the help of SQP. Due to the lack of the method for validating the optimality of a perturbed many-revolution multiple-impulse transfer, the homotopy-based approach is applied to make a comparison and mutual validation with the two-step approach. For fairness, the improved DE algorithm [25] is also applied as the optimizer for the homotopy-based approach.

Ten transfer cases are applied for the comparison, and the details are given in Appendix. 100 independent runs are implemented for both of the two approaches and the results are listed in Table 1. We can see that the minima of the two-step approach are almost the same as the ones of the homotopy-based approach for all the tens cases. The results indicate that limiting the last transfer leg to the last one revolution influences little on solving a many-revolution five-impulse rendezvous problem. Even if the true optimal solution may be missed with such a limitation, the best solution in 100 independent runs can still be very close to the true optimal one.

Moreover, Table 1 shows that the maxima of the homotopy-based approach are much smaller than the ones of the two-step approach. This result indicates that the

homotopy-based approach is more stable for solving such problems, and the solution obtained by the homotopy-based approach is expected to be closer to the optimum if only running one time. However, from Table 1 we can also see that much more time is required for the homotopy-based approach. In this study, the efficiency of achieving a near-optimal solution through many runs but not the optimization stability is more important because neither of the two approaches can guarantee to the optimum in one run, and multiple runs are necessary to produce a near-optimal solution. From this point of view, the two-step approach is more efficient.

Table 1 Optimization results of the two approaches on the test cases

Case	Approach	Maximum, m/s	Minimum, m/s	Average time, s	Case	Approach	Maximum, m/s	Minimum, m/s	Average time, s
1	Two-step	229.02	119.46	5.48	6	Two-step	195.71	177.70	5.32
	Homotopy	138.06	119.13	243.42		Homotopy	185.19	177.70	337.74
2	Two-step	299.04	244.61	5.89	7	Two-step	407.01	369.89	5.49
	Homotopy	265.68	243.90	369.92		Homotopy	379.54	369.91	388.52
3	Two-step	823.14	627.36	5.91	8	Two-step	695.37	496.21	4.88
	Homotopy	667.39	626.43	402.43		Homotopy	534.68	494.60	144.41
4	Two-step	321.97	256.99	5.90	9	Two-step	831.02	646.80	5.11
	Homotopy	270.56	256.92	473.65		Homotopy	729.23	645.70	194.62
5	Two-step	574.99	504.03	6.28	10	Two-step	588.56	479.96	5.29
	Homotopy	515.80	502.88	623.29		Homotopy	528.92	478.44	354.30

Table 2 Statistics of 20 independent tests for each case

Case	Maximum, m/s	Minimum, m/s	Mean, m/s	Standard deviation, m/s
1	120.32	119.13	119.46	0.34
2	244.96	243.40	244.09	0.46
3	628.04	626.50	626.97	0.43
4	257.66	256.93	257.02	0.16
5	504.74	502.92	503.57	0.44
6	178.37	177.68	177.80	0.19
7	370.42	369.87	369.93	0.12
8	498.56	494.59	495.95	1.46
9	649.78	645.02	647.17	1.14
10	480.98	478.44	479.79	0.68

The quality of the best solution selected from 100 independent runs is further checked still using the ten cases. 20 independent tests (each test contains 100 independent runs) are implemented for each case and the statistical results are listed in Table 2. Even though the true optimum of each case is unknown, it can be inferred from Table 2 that the best solution selected from 100 independent runs should have been very close to the true optimum. The small standard deviations indicate that the proposed optimization approach is capable of achieving near-optimal perturbed many-revolution multiple-impulse transfers.

IV. Optimal Velocity Increments of Perturbed Many-Revolution Multiple-Impulse Transfers

A multiple-impulse transfer can be essentially seen as a process to eliminate the semi-major axis difference, eccentricity difference, orbital plane angle difference and phase difference between the departure body and the rendezvous target through several maneuvers. The optimal velocity increments of a many-revolution multiple-impulse transfer are mainly determined by the first three differences because the large number of revolutions allows for the adjustment of the phase difference. The optimal velocity increments of a two-body many-revolution multiple-impulse transfer are almost constant because the first three differences are all fixed. However, it is quite different for the perturbed transfers. The RAANs of the departure body and rendezvous target are no longer constant, and the orbital plane angle difference varies with the increase of the transfer time. This can result in the possible variation of the optimal transfer velocity increments between the departure body and the rendezvous target. For better approximating optimal perturbed many-revolution multiple-impulse

transfers, how the optimal transfer velocity increments vary with the increase of the initial RAAN difference and transfer time is investigated in this section.

The transfers between the bodies with different RAAN variation rates are considered. These transfers can be generally divided into two kinds according to the variation trend of the RAAN difference between the departure body and the rendezvous target. The first kind refers to the transfers of which the RAAN difference tends to become smaller and smaller, and the second kind refers to the ones of that with opposite trend. Eight groups of transfer cases are tested, where the departure body and the rendezvous target are the same for all the cases in the eight groups. The transfers in the same group share the same initial states of the departure body and rendezvous target but different maximum transfer times. The initial orbit elements of the departure body and rendezvous target for the transfer cases in the first group are listed in Table 3. Starting from the RAAN difference of -4 deg, the departure body and the rendezvous target are propagated forward based on the perturbed dynamic model, and the initial RAAN differences of the departure body and rendezvous target are set to -3 deg, -2 deg, -1 deg, 1 deg, 2 deg, 3 deg, 4 deg, respectively, for the transfer cases in the other seven groups. The maximum transfer time increases from one day to tens of or even hundreds of days. All the transfer cases are optimized based on the optimization approach presented in Sec. III.

Table 3 Initial orbit elements of the departure body and rendezvous target for the transfer cases

	a , m	e , -	i , deg	Ω , deg	ω , deg	f , deg
Departure body	7142116.504	0.006172	98.581	96	257.367	135.368
Rendezvous target	7052562.111	0.007721	97.203	100	13.265	311.656

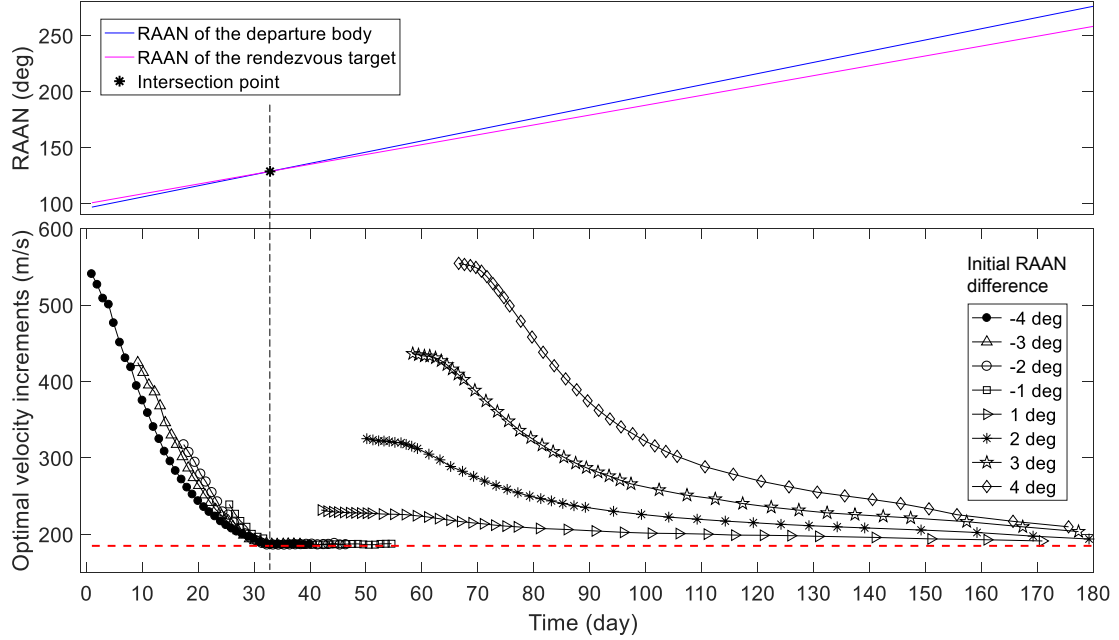


Fig. 2 Optimal velocity increments of the transfer cases with different transfer times and initial RAAN differences between the departure body and the rendezvous target

Figure 2 illustrates the optimal velocity increments of all the transfer cases in the eight groups. Each point corresponds to a transfer case (e.g., the third triangle corresponds to the case with an initial RAAN difference of -3 deg and a maximum transfer time of 3 days, and the fourth square corresponds to that with an initial RAAN difference of -1 deg and a maximum transfer time of 4 days).

Three interesting conclusions can be drawn from Figure 2.

- 1) There is a lower bound of the optimal transfer velocity increments for the perturbed many-revolution multiple-impulse transfer between any two given bodies. The lower bound is determined by the semi-major axes, eccentricities and inclinations of the departure body and rendezvous target.
- 2) For a transfer that is belonging to the first kind, supposing dt is the free flight time required for the RAAN of the departure body to catch up with that of the rendezvous target, the optimal transfer velocity increments always decrease with the

increase of the maximum transfer time if the maximum transfer time is less than dt and can reach the lower bound when the maximum transfer time is approximately equal to dt . Further enlarging the maximum transfer time contributes little to the decrease of the optimal velocity increments if the maximum transfer time is greater than dt .

3) For a transfer that is belonging to the second kind, the optimal velocity increments always decrease with the increase of the maximum transfer time and can finally approach to the lower bound as long as the transfer time is sufficient.

Some other transfer cases with different initial orbit elements of the departure body and rendezvous target are also tested, and the results are similar to the situation in Figure 2.

V. DNN-Based Method for Approximating Optimal Perturbed Many-Revolution Multiple-Impulse Transfers

Although it is impossible to analytically calculate the optimal velocity increments of a perturbed many-revolution multiple-impulse transfer, the similar variation in Sec. IV indicates that the optimal transfer velocity increments is expected to be quickly estimated with a small error using a learning-based method. The DNN-based method for approximating optimal perturbed many-revolution multiple-impulse transfers is presented in this section.

A. Implementation process

The second conclusion in Sec. IV suggests that the transfers that are belonging to the first kind can be further divided into two types according to whether the RAANs of the departure body and rendezvous target cross over the intersection point because

the transfers that are belonging to each of these two types show an obviously different variation trend of the optimal velocity increments. For better approximating optimal perturbed many-revolution multiple-impulse transfers, this kind of transfers is ultimately divided into three types, which are named as “RAAN-closing” transfers, “RAAN-intersecting” transfers and “RAAN-separating” transfers, respectively, and the estimation of the optimal velocity increments is implemented individually. The transfers that are belonging to each of the three types are illustrated in Figure 3.

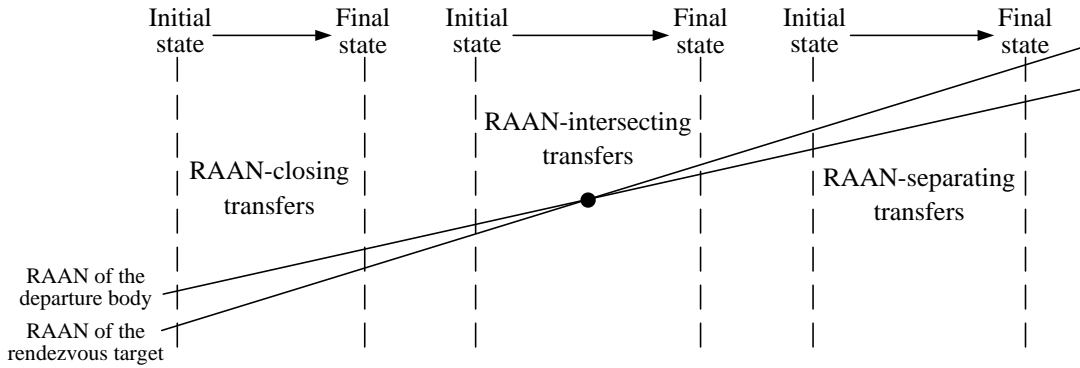


Fig. 3 Three types of perturbed many-revolution multiple-impulse transfers

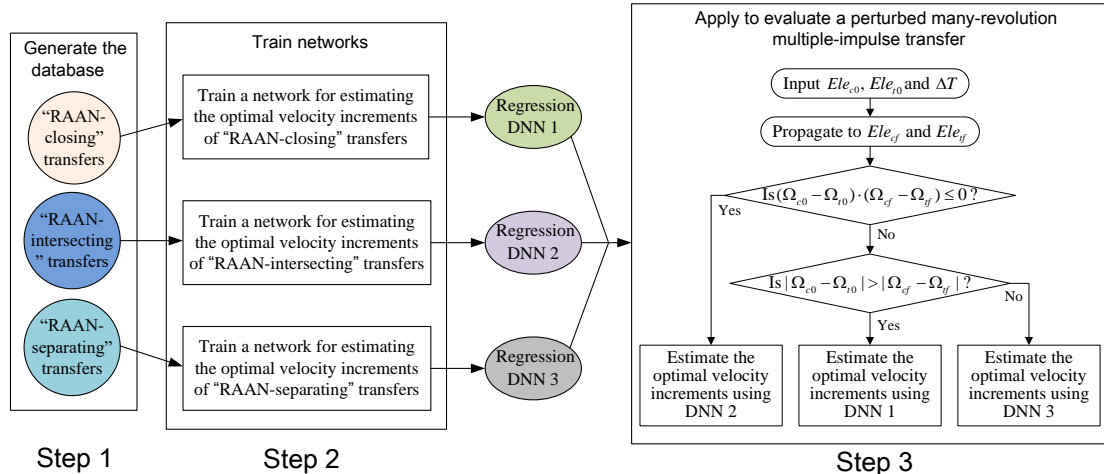


Fig. 4 Implementation process of the DNN-based method for approximating optimal perturbed many-revolution multiple-impulse transfers

The complete process of the DNN-based method for approximating optimal perturbed many-revolution multiple-impulse transfers is divided into three steps, which are illustrated in Figure 4.

The first step is to generate the database that contains three types of transfers. The samples should be generated according to the working conditions and parameter configurations for different problems.

The second step is to train three regression DNNs based on the corresponding samples. Note that the learning features and network scales of the three DNNs are determined before taking this step. The most appropriate learning features and network scales for this problem are investigated in this paper, and the results can be directly applied to similar cases when training DNNs based on the new database.

The third step is to apply the well-trained DNNs to the mission design. The flow chart for approximating the perturbed many-revolution multiple-impulse transfer between any two bodies is presented in the third step, where Ele_{c0} , Ele_{r0} , Ele_{cf} , Ele_{rf} are the initial and final orbit elements of the departure body and rendezvous target, respectively, and Ω_{c0} , Ω_{r0} , Ω_{cf} , Ω_{rf} are the initial and final RAANs of the departure body and rendezvous target, respectively.

B. Database generation method

Few “RAAN-intersecting” transfers can be obtained if generating a training sample by directly selecting two real-world central bodies and randomly determining the transfer time. To improve the efficiency of obtaining “RAAN-intersecting” transfers and balance the proportions of the three types of transfers, a more efficient method is applied to generate the database.

Algorithms 1 to 3 present the method of generating the training samples for each of the three types, where $\dot{\Omega}_c$ and $\dot{\Omega}_r$ are the RAAN variation rates of the departure

body and rendezvous target, and d_1 and d_2 are two parameters to determine the maxima of final and initial RAAN differences. This method generates a training sample by randomly producing the orbit elements of the departure body and rendezvous target first and adjust the RAAN of the rendezvous target according to that of the departure body and the transfer time. Note that the samples are not the transfers between two real-world central bodies but the ones between two virtual bodies. In fact, there is no need to use the real-world central bodies for database generation because the DNN models trained by the transfers between virtual bodies can also be applied to approximate the optimal transfers between real-world central bodies as long as they have the same parameter configuration.

Algorithm 1 Pseudocode of the process to generate an “RAAN-closing” transfer

- 1: Randomly produce Ele_{cf} , Ele_{if} and ΔT within each range according to the working situation of the problem
- 2: Calculate $\dot{\Omega}_c$ and $\dot{\Omega}_t$
- 3: Randomly produce a final RAAN difference $\Delta\Omega_f$ ($\Delta\Omega_f \in (0, d_1]$)
- 4: **if** $\dot{\Omega}_c < \dot{\Omega}_t$
 Reset $\Omega_{if} = \Omega_{cf} - \Delta\Omega_f$
else
 Reset $\Omega_{if} = \Omega_{cf} + \Delta\Omega_f$
end if
- 5: Inversely propagate Ele_{cf}, Ele_{if} to Ele_{c0}, Ele_{i0} (the propagation time is ΔT)
- 6: Optimize this sample (Ele_{c0}, Ele_{i0} and ΔT) and put into the database pool 1

Algorithm 2 Pseudocode of the process to generate an “RAAN-intersecting” transfer

- 1: Randomly produce Ele_{cm} , Ele_{tm} and ΔT within each range according to the working situation of the problem
- 2: Calculate $\dot{\Omega}_c$ and $\dot{\Omega}_t$
- 3: Randomly produce the intersecting time dt ($dt \in (0, \Delta T]$)
- 4: Reset $\Omega_{tm} = \Omega_{cm}$
- 5: Inversely propagate Ele_{cm}, Ele_{tm} to Ele_{c0}, Ele_{i0} (the propagation time is dt)
- 6: Optimize this sample (Ele_{c0}, Ele_{i0} and ΔT) and put into the database pool 2

Algorithm 3 Pseudocode of the process to generate an “RAAN-separating” transfer

- 1: Randomly produce Ele_{c0} , Ele_{i0} and ΔT within each range according to the working situation of the problem
- 2: Calculate $\dot{\Omega}_c$ and $\dot{\Omega}_t$

3: Randomly produce an initial RAAN difference $\Delta\Omega_0$ ($\Delta\Omega_0 \in (0, d_2]$)
 4: if $\dot{\Omega}_c < \dot{\Omega}_t$
 Reset $\Omega_{t0} = \Omega_{c0} + \Delta\Omega_0$
 else
 Reset $\Omega_{t0} = \Omega_{c0} - \Delta\Omega_0$
 end if
 5: Optimize this sample (Ele_{c0}, Ele_{t0} and ΔT) and put into the database pool 3

C. DNN models and network training method

A DNN is made up of large numbers of simple, highly interconnected processing nodes. Each node takes one or more inputs from other nodes and produces an output by applying an activation function over the weighted sum of these inputs. Nodes interact using weighted connections and are arranged in layers. In this study, multilayer perceptron (MLP) is selected as the architecture for the regression DNNs. The activation of a node in MLP is determined by the summation of all the weighted inputs, which can be expressed as

$$x_j = f\left(\sum_{i=1}^N w_{ij}x_i + b_j\right), \quad (9)$$

where x_j is the output of node j in the current layer, x_i is the output of node i in the previous layer, w_{ij} refers to the weight of the connection from node i to node j , b_j denotes the variable bias of node j , N is the total number of nodes in the previous layer, and f is the activation function. A Leaky Rectified Linear Unit (ReLU) [27] and a linear function are selected as the hidden-layer and output-layer activation functions, respectively.

Network training can be regarded as a process to adjust the weight vectors epoch by epoch, and the aim is to minimize the loss function. The mean squared error function F_r are used as the loss function for the regression DNNs, and is expressed as

$$F_r = \frac{1}{b} \sum_{i=1}^b (o_p(i) - o_m(i))^2 , \quad (10)$$

where b is the batch size and $o_p(i)$ is the predicted output of the network. $o_m(i)$ is the optimal velocity increments of a transfer. Cross-validation is applied in each epoch, and 90% of the data are used as training samples while the remaining 10% are used for validation. All the three regression DNNs are trained until convergence with mini-batch gradient decent and a batch size of $b = 32$. The adaptive moment (Adam) [28] technique is used to optimize the parameters of the networks. Keras [29] combined with TensorFlow [30] is applied to train the networks, where TensorFlow is the backend of Keras.

VI. Simulations

The demonstration of the DNN-based method for approximating optimal perturbed many-revolution multiple-impulse transfers is based on the mission in GTOC-9 [2].

A. Generating the database

Following the configuration in GTOC-9, ΔT_{\max} is set to 30 days. The orbit elements of the departure and rendezvous debris are all within the ranges shown in Table 4. The acceptable terminal errors are set to 1 m and 0.01 m/s.

Table 4 Ranges of the orbit elements for both the departure and rendezvous debris

a , km	e	i , deg	Ω , deg	ω , deg	f , deg
6900~7300	0~0.02	96~101	0~360	0~360	0~360

The parameters d_1 and d_2 in Algorithms 1 and 3 are both set to 10 deg. Large numbers of transfers are obtained based on the database generation method. The samples belonging to each of the three transfer types are generated individually using

Algorithms 1 to 3. One thousand transfers are randomly selected as the test samples for each problem, and the remaining ones are used as the training samples.

B. Selection of the learning features

An appropriate selection of the learning features is important because the lack of the relevant features and the interference of the redundant features both reduce the approximating performance [31]. Domain knowledge suggests that the optimal velocity increments of a perturbed many-revolution multiple-impulse transfer should relate to its initial and final states. The possible appropriate features for approximating perturbed many-revolution multiple-impulse transfers are listed in Table 5, where the first six are required features and others are alternative ones. The number of training samples is set to 5000, and a two-hidden-layer network with 30 nodes is first applied to compare the approximating performance of different feature combinations for estimating the optimal transfer velocity increments.

Table 5 Possible features for approximating perturbed many-revolution multiple-impulse transfers

Feature	Description
a_c, a_t	Semi-major axes of the departure body and rendezvous target
e_c, e_t	Eccentricities of the departure body and rendezvous target
i_c, i_t	Inclinations of the departure body and rendezvous target
$\Delta\Omega_{c0r0}$	Difference between initial RAAN of the departure body and initial RAAN of the rendezvous target
$\Delta\Omega_{cff}$	Difference between final RAAN of the departure body and final RAAN of the rendezvous target
$\Delta\Omega_{c0ff}$	Difference between initial RAAN of the departure body and final RAAN of the rendezvous target
$\dot{\Omega}_c, \dot{\Omega}_t$	RAAN variation rates of the departure body and rendezvous target
$\Delta\varphi_0, \Delta\varphi_f$	Initial and final phase differences between the departure body and rendezvous target
ΔT	Transfer time

Mean relative error (MRE) is used as the evaluation criterion and is defined as

$$\varepsilon_{\text{MRE}} = \frac{1}{N} \cdot \sum_{i=1}^N \frac{|\Delta V_{\text{Esti}}^i - \Delta V_{\text{Opti}}^i|}{\Delta V_{\text{Opti}}^i}, \quad (11)$$

where N refers to the number of testing samples; ΔV_{Esti}^i and ΔV_{Opti}^i denote the estimated and optimized optimal velocity increments of the i th transfer, respectively.

Tables 6 to 8 list the MREs of all the tested groups for the three types of transfers. The MREs of Groups 5 and 6 in Tables 6 to 8 show that $\dot{\Omega}_c$, $\dot{\Omega}_t$ and $\Delta\varphi_0$, $\Delta\varphi_f$ contribute little to the improvement of the approximating performance for all the three types of transfers. These results strongly verify that the optimal velocity increments of many-revolution multiple-impulse transfers indeed relate little to the phase difference between the departure body and the rendezvous target. The comparisons of Groups 1, 2, 3, 4 and 7 in Tables 6 and 8 show that $\Delta\Omega_{c0t0}$, $\Delta\Omega_{cftf}$ and ΔT can help improve the approximating performance for both “RAAN-closing” and “RAAN-separating” transfers, while $\Delta\Omega_{c0f}$ is helpful only when estimating the optimal velocity increments of “RAAN-separating” transfers. The comparison of Groups 1 to 7 in Table 7 verifies the correctness of the first conclusion in Sec. IV and indicates that the required features in Table 5 are sufficient to well estimate the optimal velocity increments of “RAAN-intersecting” transfers. Consequently, the combinations of Group 7 in Table 6, Group 1 in Table 7 and Group 7 in Table 8 are selected as the learning features for estimating the optimal velocity increments of the three types of transfers, respectively, and they are fixed in the following simulations. The results in these three Tables also reflect the difference of the three regression problems and

verify the reasonability and necessity of the division for perturbed many-revolution multiple-impulse transfers.

Table 6 MREs of the estimation of “RAAN-closing” transfers using different features

Group	Feature combination	MRE
1	$a_c, a_t + e_c, e_t + i_c, i_t$	46.22%
2	$a_c, a_t + e_c, e_t + i_c, i_t + \Delta\Omega_{c0t0}$	28.49%
3	$a_c, a_t + e_c, e_t + i_c, i_t + \Delta\Omega_{c0t0} + \Delta\Omega_{cff}$	12.54%
4	$a_c, a_t + e_c, e_t + i_c, i_t + \Delta\Omega_{c0t0} + \Delta\Omega_{cff} + \Delta\Omega_{c0tf}$	13.15%
5	$a_c, a_t + e_c, e_t + i_c, i_t + \Delta\Omega_{c0t0} + \Delta\Omega_{cff} + \dot{\Omega}_c, \dot{\Omega}_t$	12.51%
6	$a_c, a_t + e_c, e_t + i_c, i_t + \Delta\Omega_{c0t0} + \Delta\Omega_{cff} + \Delta\varphi_0, \Delta\varphi_f$	12.49%
7	$a_c, a_t + e_c, e_t + i_c, i_t + \Delta\Omega_{c0t0} + \Delta\Omega_{cff} + \Delta T$	5.98%

Table 7 MREs of the estimation of “RAAN-intersecting” transfers using different features

Group	Feature combination	MRE
1	$a_c, a_t + e_c, e_t + i_c, i_t$	5.95%
2	$a_c, a_t + e_c, e_t + i_c, i_t + \Delta\Omega_{c0t0}$	5.94%
3	$a_c, a_t + e_c, e_t + i_c, i_t + \Delta\Omega_{c0t0} + \Delta\Omega_{cff}$	6.04%
4	$a_c, a_t + e_c, e_t + i_c, i_t + \Delta\Omega_{c0t0} + \Delta\Omega_{c0tf}$	6.09%
5	$a_c, a_t + e_c, e_t + i_c, i_t + \Delta\Omega_{c0t0} + \dot{\Omega}_c, \dot{\Omega}_t$	5.99%
6	$a_c, a_t + e_c, e_t + i_c, i_t + \Delta\Omega_{c0t0} + \Delta\varphi_0, \Delta\varphi_f$	5.97%
7	$a_c, a_t + e_c, e_t + i_c, i_t + \Delta\Omega_{c0t0} + \Delta T$	6.00%

Table 8 MREs of the estimation of “RAAN-separating” transfers using different features

Group	Feature combination	MRE
1	$a_c, a_t + e_c, e_t + i_c, i_t$	44.54%
2	$a_c, a_t + e_c, e_t + i_c, i_t + \Delta\Omega_{c0t0}$	14.64%
3	$a_c, a_t + e_c, e_t + i_c, i_t + \Delta\Omega_{c0t0} + \Delta\Omega_{cff}$	11.25%
4	$a_c, a_t + e_c, e_t + i_c, i_t + \Delta\Omega_{c0t0} + \Delta\Omega_{cff} + \Delta\Omega_{c0tf}$	8.54%
5	$a_c, a_t + e_c, e_t + i_c, i_t + \Delta\Omega_{c0t0} + \Delta\Omega_{cff} + \Delta\Omega_{c0tf} + \dot{\Omega}_c, \dot{\Omega}_t$	8.53%
6	$a_c, a_t + e_c, e_t + i_c, i_t + \Delta\Omega_{c0t0} + \Delta\Omega_{cff} + \Delta\Omega_{c0tf} + \Delta\varphi_0, \Delta\varphi_f$	8.52%
7	$a_c, a_t + e_c, e_t + i_c, i_t + \Delta\Omega_{c0t0} + \Delta\Omega_{cff} + \Delta\Omega_{c0tf} + \Delta T$	5.51%

C. Determination of the network and training data scales

An appropriate scale of the network is necessary to avoid underfitting and overfitting. Different numbers of hidden layers and nodes are tested to determine the most appropriate scales for the three regression problems.

Figures 5 to 7 illustrate the MREs of the estimations with the number of hidden layers varying from two to four and the number of nodes in each layer varying from 10 to 100. It is shown that a network scale of 2×60 is appropriate for estimating the optimal velocity increments of “RAAN-intersecting” transfers. However, larger scales are required for the other two types of transfers, where 3×60 and 3×70 should be the best choices, respectively. Figure 8 illustrates the decreases in the MREs as the number of training samples increases from 2×10^3 to 10^5 . The results show that the MREs of the estimations for the three types of transfers can all be decreased to less than 3% with sufficient training samples. 5×10^4 samples is enough to converge to the near-best approximating performance when estimating the optimal velocity increments of “RAAN-intersecting” transfers, while at least 7×10^4 and 8×10^4 samples are required for “RAAN-closing” and “RAAN-separating” transfers, respectively. The requirement of larger network and training data scales indicates that estimating the optimal velocity increments for an “RAAN-closing” or “RAAN-separating” transfer is more difficult than that for an “RAAN-intersecting” transfer.

Due to the unavoidable errors between the training samples and the corresponding true-optimal transfers and the possible systematic noise of these learning problems, further enlarging the training data scale makes no significant contribution to improvement in the approximating performance. Nevertheless, such an approximating performance is competent for application to the preliminary design of a perturbed multiple-impulse-based multitarget rendezvous mission.

Moreover, we notice that some participants of GTOC-9 including the champion team Jet Propulsion Laboratory (JPL) have created a database for quick lookups for approximating the optimal transfers between any two pieces of debris [3, 6]. Billions of debris-to-debris transfers are required to approximately cover the whole search space. While only tens of thousands of training samples are sufficient to approximate the optimal transfers with an acceptable estimation error by means of the DNN-based method. This comparison strongly shows the advantage of the DNN-based method for application to real-world problems.

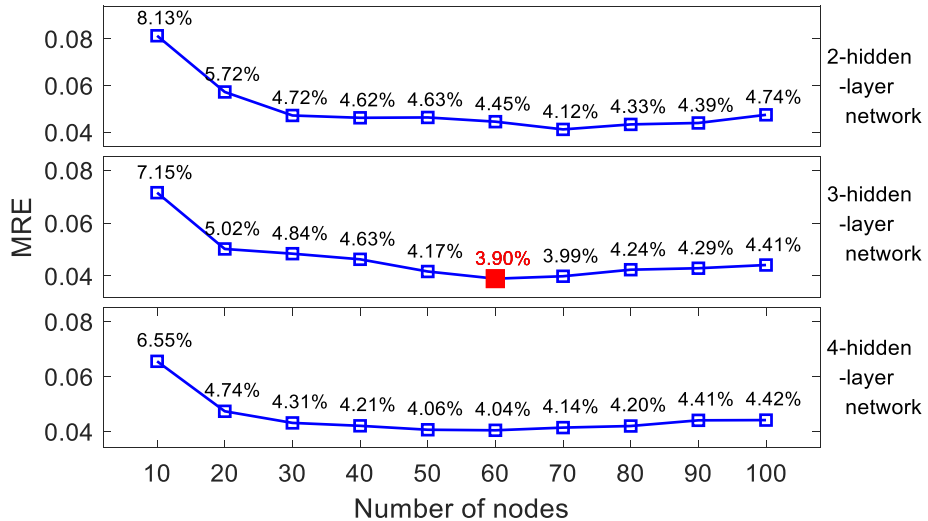


Fig. 5 MREs of the estimation of “RAAN-closing” transfers for networks with different numbers of hidden layers and nodes

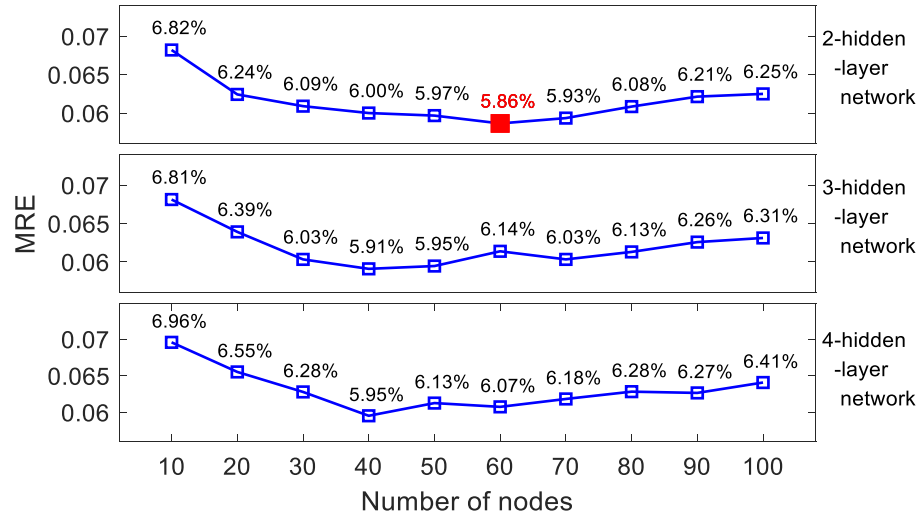


Fig. 6 MREs of the estimation of “RAAN- intersecting” transfers for networks with different numbers of hidden layers and nodes

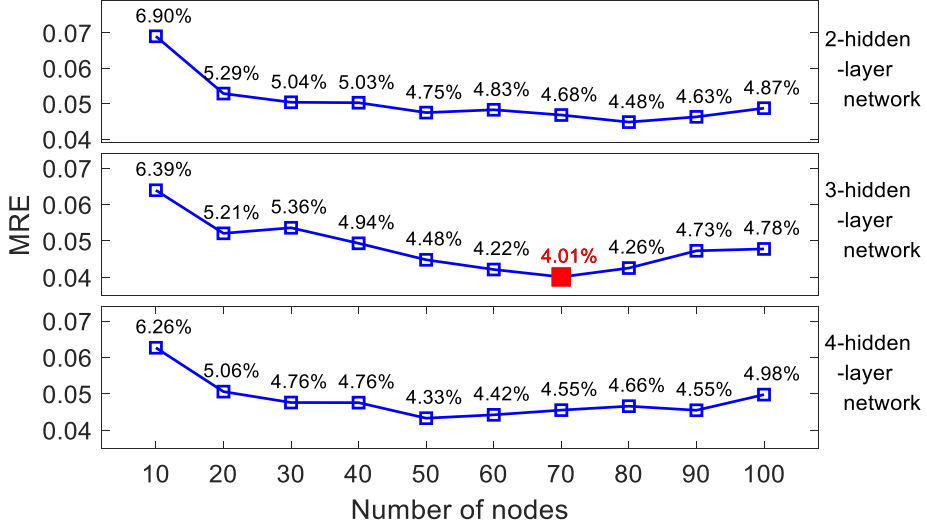


Fig. 7 MREs of the estimation of “RAAN-separating” transfers for networks with different numbers of hidden layers and nodes

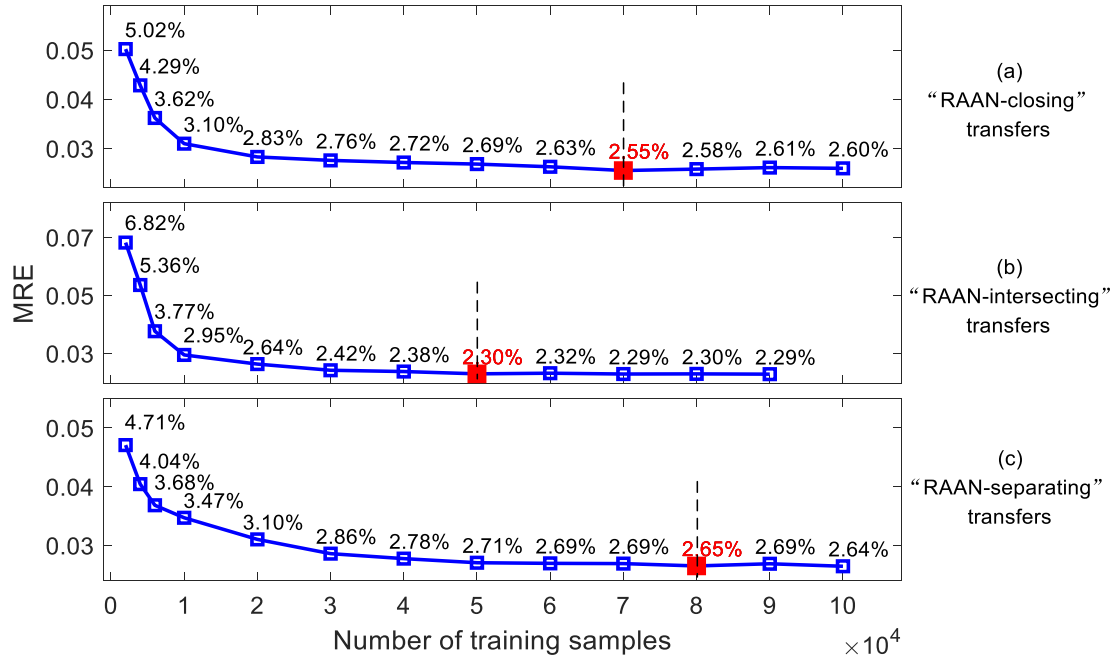


Fig. 8 MREs of the estimation with different training data scales for the three types of transfers

D. Comparison with analytical estimation methods

Two typical analytical estimation methods for approximating optimal perturbed many-revolution multiple-impulse transfers are compared with the DNN-based method. The first method developed based on the Gauss form of variational equations [32] is proposed by the National University of Defense Technology (NUDT) team,

and the second method that is similar to the Edelbaum's method for approximating high-thrust transfers [33] is proposed by the Xi'an Satellite Control Center (XSCC) team. Detailed procedures of the two methods can be seen in [4] and [5]. For convenience, they are named as NUDT method and XSCC method.

The estimation results of the test samples obtained by the two analytical methods and the DNN-based method are all listed in Table 9. It can be seen from Table 9 that both the NUDT method and the XSCC method perform much worse than the DNN-based method on the approximation of all the three types of transfers. Due to the lack of the consideration of necessary features such as the transfer time, the MREs of the two analytical methods can be as high as over 20% when estimate the optimal velocity increments of “RAAN-closing” and “RAAN-separating” transfers. Figure 9 further visualizes the statistics of the estimation error of the three methods. We can find that the distributions of the estimation error obtained by the two analytical methods are much wider than those obtained by the DNN-based method for all the three types of transfers, and the centers of the distributions obtained by the two analytical methods all deviate from 0. These results indicate that there are not only larger random errors but also systematic errors when estimating the optimal velocity increments of the three types of transfers using either the NUDT method or the XSCC method. This comparison strongly shows the superiority of the DNN-based method for quickly approximating optimal perturbed many-revolution multiple-impulse transfers.

Table 9 MREs of the estimation for the two analytical methods and DNN-based method

	“RAAN-closing” transfers	“RAAN-intersecting” transfers	“RAAN-separating” transfers
NUDT method	20.37%	17.93%	20.82%
XSCC method	21.96%	16.28%	22.43%
DNN-based method	2.56%	2.29%	2.64%

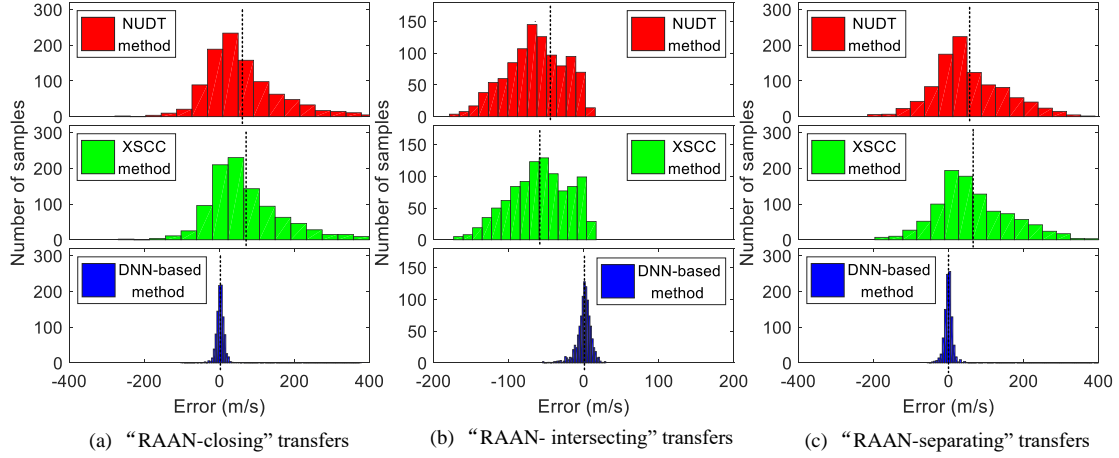


Fig. 9 Error distributions of the tested samples obtained by the two analytical methods and DNN-based method

E. Verification on debris transfer chains

To verify the efficiency of the DNN-based method for real-world applications, the fast approximation of successive transfers is further studied. Two transfer chains that were achieved by the JPL team in GTOC-9 are selected as the test cases [3], where a total of 14 and 12 pieces of debris are contained in Chain 1 and Chain 2, respectively. The debris IDs, as well as the departure time, rendezvous time and accumulative velocity increments of each transfer are listed in Table 10. The epoch data of the debris can be accessed on GTOC Portal [34].

The DNN-estimated velocity increments of the two transfer chains are illustrated in Figures 10 and 11. The results obtained by the NUDT method and the XSCC method are also presented for comparison. It can be seen from Table 10 and Figures 10 and 11 that the estimation errors of the two analytical methods keep increasing transfer by

transfer and finally reach the extreme values (over 300 m/s and 400 m/s for the NUDT method and the XSCC method, respectively). The systematic error shown in Figure 9 causes the accumulation of the estimation error and results in a larger and larger deviation between the estimated accumulative velocity increments and the true accumulative velocity increments. Without the interference of the systematic error and because of the offset of all the random error, the total velocity increments estimated by the DNN-based method can fit the true value very well for both chains and obtain the final results with very small errors (approximately 9 m/s and 8 m/s for Chain 1 and Chain 2, respectively). The comparisons in these two cases further show the significant advantage of the DNN-based method for approximating optimal perturbed many-revolution multiple-impulse transfers, especially for the approximation of successive transfers.

Table 10 Transfer chains in GTOC-9 obtained by JPL

Transfer Chain 1				Transfer Chain 2			
Debris ID	Rendezvous time, MJD2000	Departure time, MJD2000	Accumulative ΔV , m/s	Debris ID	Rendezvous time, MJD2000	Departure time, MJD2000	Accumulative ΔV , m/s
23	—	23557.18	0	33	—	25951.06	0
55	23587.04	23592.04	161.8	68	25973.75	25979.26	83.3
79	23617.02	23622.06	301.0	116	25983.50	25989.03	231.4
113	23644.48	23649.49	366.8	106	26013.50	26019.03	727.3
25	23674.48	23679.49	575.0	14	26043.49	26049.02	1192.2
20	23679.78	23684.81	690.2	52	26073.49	26079.04	1597.4
27	23695.44	23700.44	990.3	120	26103.48	26109.02	1883.3
117	23725.44	23730.44	1555.2	80	26133.48	26139.01	2138.1
121	23733.14	23738.14	1633.5	16	26163.47	26169.01	2200.4
50	23739.65	23744.68	1738.5	94	26193.47	26199.02	2357.0
95	23746.09	23751.12	1971.8	83	26217.56	26223.08	2393.5
102	23775.79	23780.83	2425.3	89	26232.30	—	2568.4
38	23805.14	23810.18	2765.7				
97	23816.04	—	3066.5				

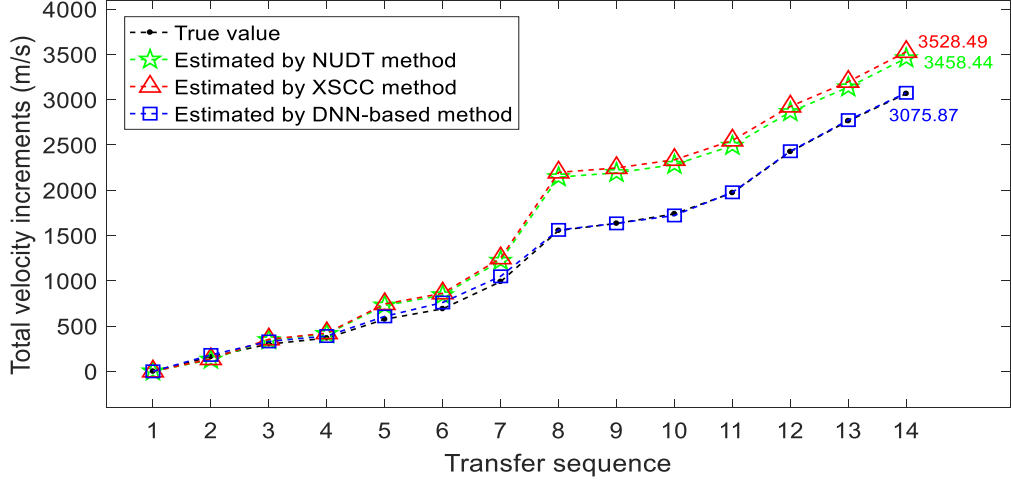


Fig. 10 True and estimated total velocity increments of Chain 1

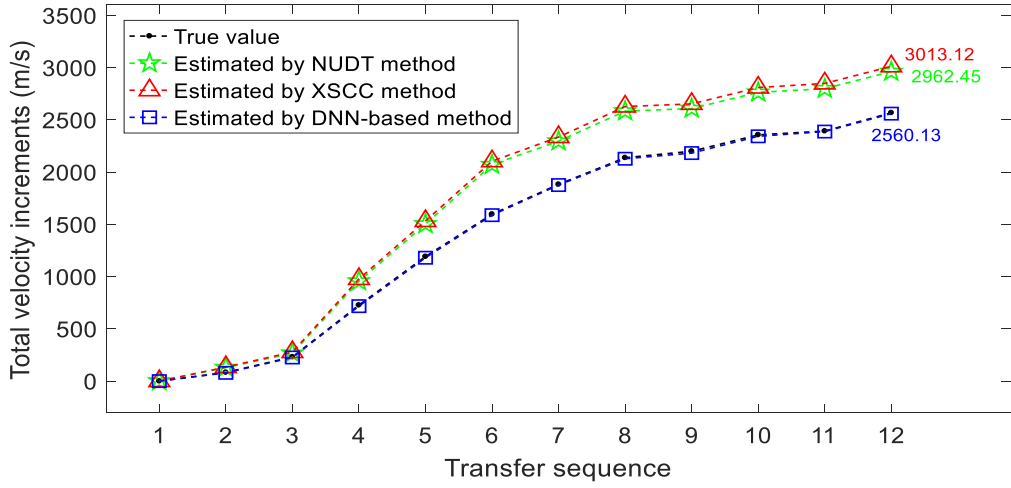


Fig. 11 True and estimated total velocity increments of Chain 2

VII. Conclusions

Fast approximation of optimal perturbed many-revolution multiple-impulse transfers is studied in this paper. A two-step optimization approach for obtaining near-optimal transfers is first developed, and the efficiency of the approach is validated. How the optimal transfer velocity increments vary with the increase of the initial RAAN difference and transfer time is investigated, and the result indicates that perturbed many-revolution multiple-impulse transfers should ultimately be divided into three types of transfers. A DNN-based method for quickly approximating optimal perturbed many-revolution multiple-impulse transfers is proposed, where three

regression DNNs are required to estimate the optimal velocity increments of each type of transfers. The implementation process of the DNN-based method as well as the methods for generating the database and training the regression DNNs are presented. The most appropriate learning features and network scales for estimating the optimal velocity increments of each type of transfers are determined, and the superiority and reliability of the DNN-based method for quickly estimating the optimal velocity increments are shown by comparison with two typical analytical estimation methods. The case study on two debris transfer chains further reveals the advantage of the DNN-based method for estimating the optimal velocity increments for successive perturbed many-revolution multiple-impulse transfers.

Acknowledgments

This work was supported by the Natural Science Foundation of China (11572345).

Appendix

The initial orbital elements of the departure bodies and rendezvous targets as well as the maximum transfer times of the ten test cases in Sec. III are listed in Table 11.

Table 11 Ten transfer cases for testing the efficiency of the two-step approach

Case	Classic orbital elements, (m, -, deg, deg, deg, deg)		Maximum transfer time, day
	Departure body	Rendezvous target	
1	[7102019.008, 0.0033, 98.173, 1.258, 188.448, 221.186]	[7113158.741, 0.0133, 98.524, 0, 164.332, 65.562]	9.724
2	[7042245.022, 0.0059, 99.277, 5.268, 252.645, 259.213]	[7004095.428, 0.0151, 100.634, 0, 298.769, 222.769]	19.989
3	[6996726.169, 0.0138, 99.902, 0, 359.571, 135.360]	[7064707.883, 0.0199, 96.367, 15.449, 305.414, 246.734]	23.463
4	[6995199.808, 0.0081, 99.515, 0, 270.585, 350.836]	[7239184.088, 0.0096, 97.791, 7.218, 32.369, 200.043]	22.202
5	[7280713.695, 0.0028, 100.420, 0, 264.779, 228.623]	[7110280.222, 0.0134, 96.592, 9.866, 286.569, 273.241]	28.049
6	[7207996.616, 0.0007, 99.455, 0, 320.522, 22.026]	[7283641.352, 0.0049, 98.135, 2.725, 337.486, 227.488]	15.081

7	[7147223.604, 0.0067, 99.207, 0, 276.253, 27.814]	[7008415.946, 0.0063, 96.439, 4.885, 334.205, 20.624]	18.306
8	[6963079.862, 0.0194, 97.666, 0, 184.209, 319.741]	[6933400.666, 0.0028, 97.900, 3.691, 288.044, 283.661]	2.582
9	[7151921.596, 0.0156, 96.485, 0, 20.478, 43.734]	[6977324.893, 0.0067, 96.184, 3.776, 233.778, 276.058]	5.481
10	[6991377.623, 0.0027, 99.166, 4.705, 50.878, 200.219]	[7132670.622, 0.0199, 96.617, 0, 88.349, 171.312]	16.876

References

[1] Helvig, C. S., Robins, G., and Zelikovsky, A., “The moving-target traveling salesman problem,” *Journal of Algorithms*, Vol. 49, No. 1, 2003, pp. 153-174.
[doi: 10.1016/S0196-6774\(03\)00075-0](https://doi.org/10.1016/S0196-6774(03)00075-0)

[2] Dario, I., and Marcus, M., “The Kessler Run: On the Design of the GTOC9 Challenge,” *Acta Futura*, Vol. 11, 2018, pp. 11-24.
[doi: 10.5281/zenodo.1139022](https://doi.org/10.5281/zenodo.1139022)

[3] Anastassios, P., Daniel, G., Drew, J., Gregory, L., Austin, N., Javier, R., Juan, S., Jeffrey, S., Nitin, A., Thomas, P., Try, L., Timothy, M., Ralph, R., David, G., Nicholas, B., Damon, L., Zahi, T., Frank, L., Eugene, B., Mark, W., and Jon, S., “GTOC9: Results from the Jet Propulsion Laboratory (team JPL),” *Acta Futura*, Vol. 11, 2018, pp. 25-35.
[doi: 10.5281/zenodo.1139152](https://doi.org/10.5281/zenodo.1139152)

[4] Luo, Y. Z., Zhu, Y. H., Zhu, H., Yang, Z., Sun, Z. J., and Zhang, J., “GTOC9: Results from the National University of Defense Technology (team NUDT),” *Acta Futura*, Vol. 11, 2018, pp. 37-47.
[doi: 10.5281/zenodo.1139226](https://doi.org/10.5281/zenodo.1139226)

[5] Shen, H. X., Zhang, T. J., Huang, A. Y., and Li, Z., “GTOC9: Results from the Xi'an Satellite Control Center (team XSCC),” *Acta Futura*, Vol. 11, 2018, pp. 49-55.
[doi: 10.5281/zenodo.1139240](https://doi.org/10.5281/zenodo.1139240)

[6] Enrico, B., Francesco, B., and Matteo, R., “GTOC9: Results from University of Trento (team ELFMAN),” *Acta Futura*, Vol. 11, 2018, pp. 79-90.
[doi: 10.5281/zenodo.1139258](https://doi.org/10.5281/zenodo.1139258)

[7] Nathan, L. P., Daniel, J. S., Simon, T., Chandrakanth, V., Jonathan, A., Marielle, P., Oscar, F., and Stijn, D. S., “GTOC 9: Results from the University of Colorado at Boulder (team CU Boulder),” *Acta Futura*, Vol. 11, 2018, pp. 91-97.
[doi: 10.5281/zenodo.1139268](https://doi.org/10.5281/zenodo.1139268)

[8] Huang, G. B., Zhou, H., Ding, X., and Zhang, R., “Extreme learning machine for regression and multiclass classification,” *IEEE Transactions on Systems Man & Cybernetics Part B*, Vol. 42, No. 2, 2012, pp. 513-529.
[doi: 10.1109/tsmc.2011.2168604](https://doi.org/10.1109/tsmc.2011.2168604)

[9] Shang, H., and Liu, Y., “Assessing Accessibility of Main-Belt Asteroids Based on Gaussian Process Regression,” *Journal of Guidance Control Dynamics*, Vol. 40, No. 5, 2017, pp. 1-11.
[doi: 10.2514/1.G000576](https://doi.org/10.2514/1.G000576)

[10] Zhu, Y. H., Luo, Y. Z., and Yao, W., “Fast Accessibility Evaluation of the Main-Belt Asteroids Manned Exploration Mission Based on a Learning Method,” *IEEE Congress on Evolutionary Computation*, Rio de Janeiro, 2018, pp. 1-8.
doi: 10.1109/CEC.2018.8477849

[11] Hennes, D., Izzo, D., and Landau, D., “Fast approximators for optimal low-thrust hops between main belt asteroids,” *Computational Intelligence*, 2017.
doi: 10.1109/SSCI.2016.7850107

[12] Mereta, A., Izzo, D., and Wittig, A., “Machine Learning of Optimal Low-Thrust Transfers Between Near-Earth Objects,” *International Conference on Hybrid Artificial Intelligence Systems*, 2017, pp. 543-553.
10.1007/978-3-319-59650-1_46

[13] Lecun, Y., Bengio, Y., and Hinton, G., “Deep learning,” *Nature*, Vol. 521, No. 7553, 2015, p. 436.
doi: 10.1038/nature14539

[14] Schmidhuber, J., “Deep learning in neural networks: An overview,” *Neural Networks*, Vol. 61, 2015, pp. 85-117.
doi: 10.1016/j.neunet.2014.09.003

[15] Silver, D., Huang, A., Maddison, C. J., Guez, A., Sifre, L., Driessche, G. V. D., Schrittwieser, J., Antonoglou, I., Panneershelvam, V., and Lanctot, M., “Mastering the game of Go with deep neural networks and tree search,” *Nature*, Vol. 529, No. 7587, 2016, pp. 484-489.
doi: 10.1038/nature16961

[16] Fernandez, J. M. F., and Mahlmann, T., “The Dota 2 Bot Competition,” *IEEE Transactions on Games*, Vol. PP, No. 99, 2018, pp. 1-1.
doi: 10.1109/TG.2018.2834566

[17] Sánchez-Sánchez, C., and Izzo, D., “Real-time optimal control via Deep Neural Networks: study on landing problems,” *Journal of Guidance Control & Dynamics*, Vol. 41, No. 3, 2018, pp. 1-14.
doi: 10.2514/1.G002357

[18] Sanchez-Sanchez, C., Izzo, D., and Hennes, D., “Learning the optimal state-feedback using deep networks,” *Computational Intelligence*, 2017.
doi: 10.1109/SSCI.2016.7850105

[19] Maggiori, E., Tarabalka, Y., Charpiat, G., and Alliez, P., “Convolutional Neural Networks for Large-Scale Remote-Sensing Image Classification,” *IEEE Transactions on Geoscience & Remote Sensing*, Vol. 55, No. 2, 2016, pp. 645-657.
doi: 10.1109/TGRS.2016.2612821

[20] Furfaro, R., Bloise, I., Orlandelli, M., Di Lizia, P., Topputo, F., and Linares, R., “A Recurrent Deep Architecture for Quasi-Optimal Feedback Guidance in Planetary Landing,” *IAA SciTech Forum on Space Flight Mechanics and Space Structures and Materials*, 2018, pp. 1-24.

[21] Peng, H., and Bai, X., “Artificial Neural Network-Based Machine Learning Approach to Improve Orbit Prediction Accuracy,” *Journal of Spacecraft and Rockets*, 2018, pp. 1-13.
doi: 10.2514/6.2018-1966

[22] Prussing, J. E., and Chiu, J. H., “Optimal multiple-impulse time-fixed rendezvous between circular orbits,” *Journal of Guidance Control & Dynamics*, Vol. 9, No. 1, 2012, pp. 77-81.
doi: 10.2514/3.20060

[23] Battin, R. H. *An Introduction to the Mathematics and Methods of Astrodynamics*: AIAA, 1999.

[24] Shenand, H., and Tsotras, P., "Optimal Two-Impulse Rendezvous Using Multiple-Revolution Lambert Solutions," *Journal of Guidance Control & Dynamics*, Vol. 26, No. 1, 2003, pp. p ágs. 50-61.
doi: 10.2514/2.5014

[25] Zhu, Y., Luo, Y., and Jin, Z., "Packing programming of space station spacewalk events based on bin packing theory and differential evolution algorithm," *IEEE Congress on Evolutionary Computation*, Vancouver, 2016, pp. 877-884.
doi: 10.1109/CEC.2016.7743883

[26] Yang, Z., Luo, Y. Z., Zhang, J., and Tang, G. J., "Homotopic Perturbed Lambert Algorithm for Long-Duration Rendezvous Optimization," *Journal of Guidance Control & Dynamics*, Vol. 38, No. 11, 2015, pp. 1-9.
doi: 10.2514/1.g001198

[27] Karlik, B., and Olgac, A. V., "Performance analysis of various activation functions in generalized MLP architectures of neural networks," *International Journal of Artificial Intelligence and Expert Systems*, Vol. 1, No. 4, 2011, pp. 111-122.

[28] Ruder, S., "An overview of gradient descent optimization algorithms," 2016.
arXiv:1609.04747

[29] Chollet, F., "Keras: The Python Deep Learning library," 2016.
https://keras.io/

[30] Abadi, M., Barham, P., Chen, J., Chen, Z., Davis, A., Dean, J., Devin, M., Ghemawat, S., Irving, G., and Isard, M., "TensorFlow: A system for large-scale machine learning," 2016.

[31] Bing, X., Zhang, M., Browne, W., and Xin, Y., "A Survey on Evolutionary Computation Approaches to Feature Selection," *IEEE Transactions on Evolutionary Computation*, Vol. 20, No. 4, 2016, pp. 606-626.
doi: 10.1109/TEVC.2015.2504420

[32] Luo, Y. Z., Li, H. Y., and Tang, G. J., "Hybrid Approach to Optimize a Rendezvous Phasing Strategy," *Journal of Guidance Control & Dynamics*, Vol. 30, No. 1, 2007, pp. 185-191.
doi: 10.2514/1.20232

[33] Edelbaum, T. N., "Propulsion requirements for controllable satellites," *Ars Journal*, Vol. 31, No. 8, 1961, pp. 1079-1089.
doi: doi:10.2514/8.5723

[34] GTOC Portal. https://sophia.estec.esa.int/gtoc_portal/.